

Journal Name

RSCPublishing

Electronic Supplementary Information

Conformable on-skin supercapacitor-integrated, strain sensor based on multioxidant-functionalized thermoplastic polyurethane/reduced graphene oxide/polypyrrole composite films

Daedong Park^a, Samayanan Selvam^{a,b*}, Jin-Heong Yim^{a*}

^aDivision of Advanced Materials Engineering, Kongju National University, Budaedong 275, Seobuk-gu, Cheonan-si, Chungnam 31080, South Korea

^bBioMe Live Analytical Centre, Karaikudi-630003

E-mail: jhyim@kongju.ac.kr; sselvam222@gmail.com;

1. Experimental details

1.1. Materials and reagents

Thermoplastic polyurethane (TPU, Dongsung, Neothane 5285AP, density: 1.19 g/cm³), which is a hydrophilic elastomer as a substrate, reduced graphene oxide (rGO, Grapheneall, carbon=92 %, D/G ratio=0.99) as a conductive carbon material, pyrrole (Acros Organics) as a conductive polymer monomer, iron(III) benzene sulfonate (A0), iron(III) *p*-toluenesulfonate (A1), iron(III) 4-ethylbenzenesulfonate (A2) synthesized with an oxidizing agent used in synthesizing a conductive polymer, tetrahydrofuran (THF, Samchun chemical) was used as a solvent.

1.2. Fabrication of TPU-rGO-PPy composite films

In the case of the TPU-rGO composite film, 10 wt% of TPU was stirred and dissolved in THF for 4 h, followed by 3 wt% of rGO and stirred for 30 minutes, and ultrasonic treatment was performed for 2 h

for uniform dispersion of rGO. After pouring the solution into the glass dish, a hole was drilled and covered using an aluminum foil to prevent the solvent from being quickly evaporated and dried, and then the solvent was completely removed and cut to a width of 10 mm and a length of 40 mm.

In the case of a TPU-rGO-PPy composite film, the TPU-rGO-PPy composite film is prepared in the same manner as in the above process after stirring strongly in THF for 2 h, followed by stirring strongly and strongly, followed by stirring. The dried composite film was subjected to Pyrrole as conductive polymer monomers and a TPU-rGO-oxidant composite film in a reactor for gas phase polymerization, and 6 mL/s of nitrogen was flowed there into to prevent additional reaction. After vapor polymerization at 25°C for 30 min, the composite film was completed by removing unreacted oxidants and other impurities remaining on the film by washing with ethanol for 30 min.

1.3. Characterization

Morphological characteristics were measured by coating TPU-rGO-PPy composite film with Pt/Au and observing it at various magnifications under 10 kV voltage using Field emission scanning electron microscopy (FE-SEM, MIRA2, TESCAN), and point analysis using energy dispersive X-ray spectroscopy (EDS, X-flash4010, Bruker) was used to confirm PPy synthesis, and X-ray photoelectron spectroscopy (XPS, K-Alpha, Thermo Fisher Scientific) was used. Physical characteristics analysis at a tensile speed of 10 mm/min using a universal testing machine (UTM, Hounsfield, H10KS) was performed, tensile-contraction was repeated at a rate of 0.08 Hz using a self-produced multi-propose flexibility test machine (IPEN Co., Korea) to change durability, reproducibility, and various strain levels, and relative electrical resistance in the DCR film was measured with a connected inductance/capability (LCR) meter. To measure performance as a supercapacitor using Workstarion (SP-150, biological), cyclic voltammetry (CV) at various scan rates (10-200 mV/s) using 1M KOH basic electrolyte, at various current densities (0.25 to 1.00 mA), constant current charge-discharge (CD), electrochemical impedance spectroscopy

(EIS) at a frequency of 100 kHz and an AC amplitude of 5 mV, I-V curves were analyzed under -10 to 10 V.

2. Results and discussions

2.1. X-ray photoelectron spectroscopy (XPS) studies

The chemical compositions and strength of the obtained TPU/rGO/PPy composite films were further examined (Fig.S1). The N1s XPS spectrum employed to confirm the synthesis of PPy in the TPU-rGO-PPy composite film. All the composite films exhibited the peaks of N-H bonds around 399 eV. Regarding TPU-rGO (Fig. S1a), when GO was reduced into rGO, the peak corresponding to residual hydrazine appeared at 400 eV, and the peaks of the main chain of the polymerized PPy and hydrazine strongly observed (Figs. S1(b-d)). Further, Table S1 summarizes the results of the elemental analysis (energy-dispersive spectroscopy, EDS) of the TPU-rGO-PPy composite films. TPU and the TPU-rGO films comprise ~78% carbon, ~17% oxygen, ~3% nitrogen, and trace amounts of sulfur and iron. Regarding the TPU-rGO-PPy films, considering that PPy was polymerized inside the film, the proportion of nitrogen increased thus: A0, 7.96%; A1, 5.34%; and A2: 4.95%. A three-dimensional disorder was observed when the polymerization was performed employing an oxidant comprising a long alkyl group; moreover, since the alkyl group, which is an electron donor, interferes with polymerization and polymerizes smaller amounts of PPy particles simultaneously, it causes a difference in the nitrogen content, and a trace amount of the oxidants that cannot be completely removed persisted. Thus, the result demonstrated the successful polymerization of the composite film employing VPP by including an oxidizing agent therein during the preparation of the conductive polymer elastomer composite.

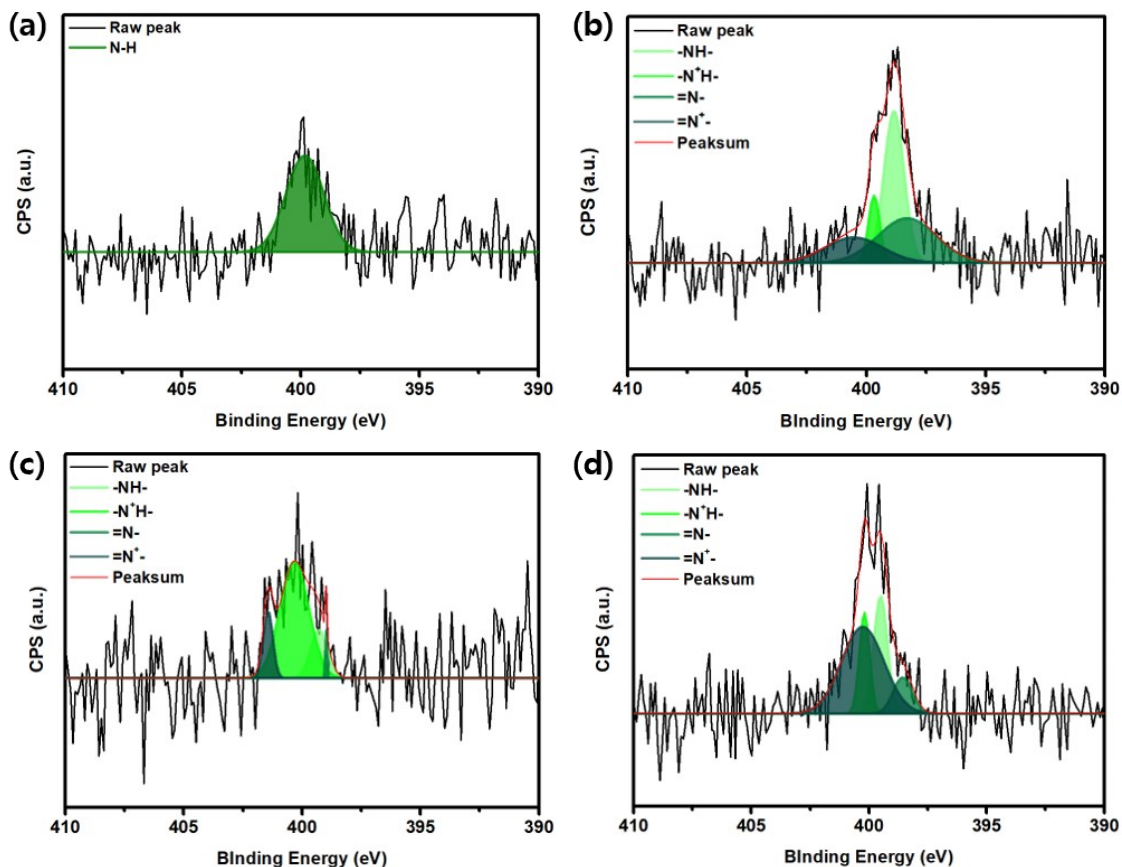


Fig.S1. XPS spectra (N1s) of the TPU-rGO-PPy composite films: (a) TPU-rGO, (b) TPU-rGO-PPy (A0), (c) TPU-rGO-PPy (A1), and (d) TPU-rGO-PPy (A2)

2.2. Energy-dispersive spectroscopy studies

Further, Table S1 summarizes the results of the elemental analysis (energy-dispersive spectroscopy, EDS) of the TPU-rGO-PPy composite films. TPU and the TPU-rGO films comprise ~78% carbon, ~17% oxygen, ~3% nitrogen, and trace amounts of sulfur and iron. Regarding the TPU-rGO-PPy films, considering that PPy was polymerized inside the film, the proportion of nitrogen increased thus: A0, 7.96%; A1, 5.34%; and A2: 4.95%. A three-dimensional disorder was observed when the polymerization was performed employing an oxidant comprising a long alkyl group; moreover, since the alkyl group, which is an electron donor, interferes with polymerization and polymerizes smaller amounts of PPy particles simultaneously, it causes a

difference in the nitrogen content, and a trace amount of the oxidants that cannot be completely removed persisted. Thus, the result demonstrated the successful polymerization of the composite film employing VPP by including an oxidizing agent therein during the preparation of the conductive polymer elastomer composite.

Tab. S1. EDS element analysis of TPU-rGO-PPy composite films

	C (at.%)	N (at.%)	O (at.%)	S (at.%)	Fe (at.%)
TPU	78.62	3.58	17.23	0.28	0.29
TPU/rGO	78.68	4.37	16.55	0.23	0.16
TPU/rGO/PPy(A0)	72.95	7.96	18.07	1.02	0.00
TPU/rGO/PPy(A1)	72.08	5.34	22.10	0.45	0.04
TPU/rGO/PPy(A2)	70.71	4.95	23.42	0.91	0.00

2.3. Surface morphology analysis

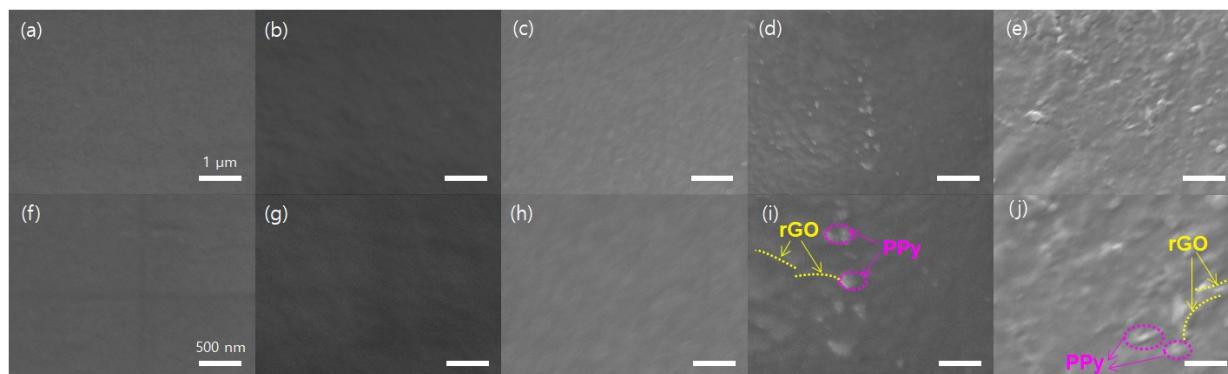


Fig. S2. Field-emission scanning electron microscopy (FE-SEM) analysis of the TPU-rGO-PPy composite films: (a, f) TPU, (b, g) TPU-rGO, (c, h) TPU-rGO-PPy (A0), (d, i) TPU-rGO-PPy (A1), and (e, j) TPU-rGO-PPy (A2).

2.4. Mechanical Properties of composite films

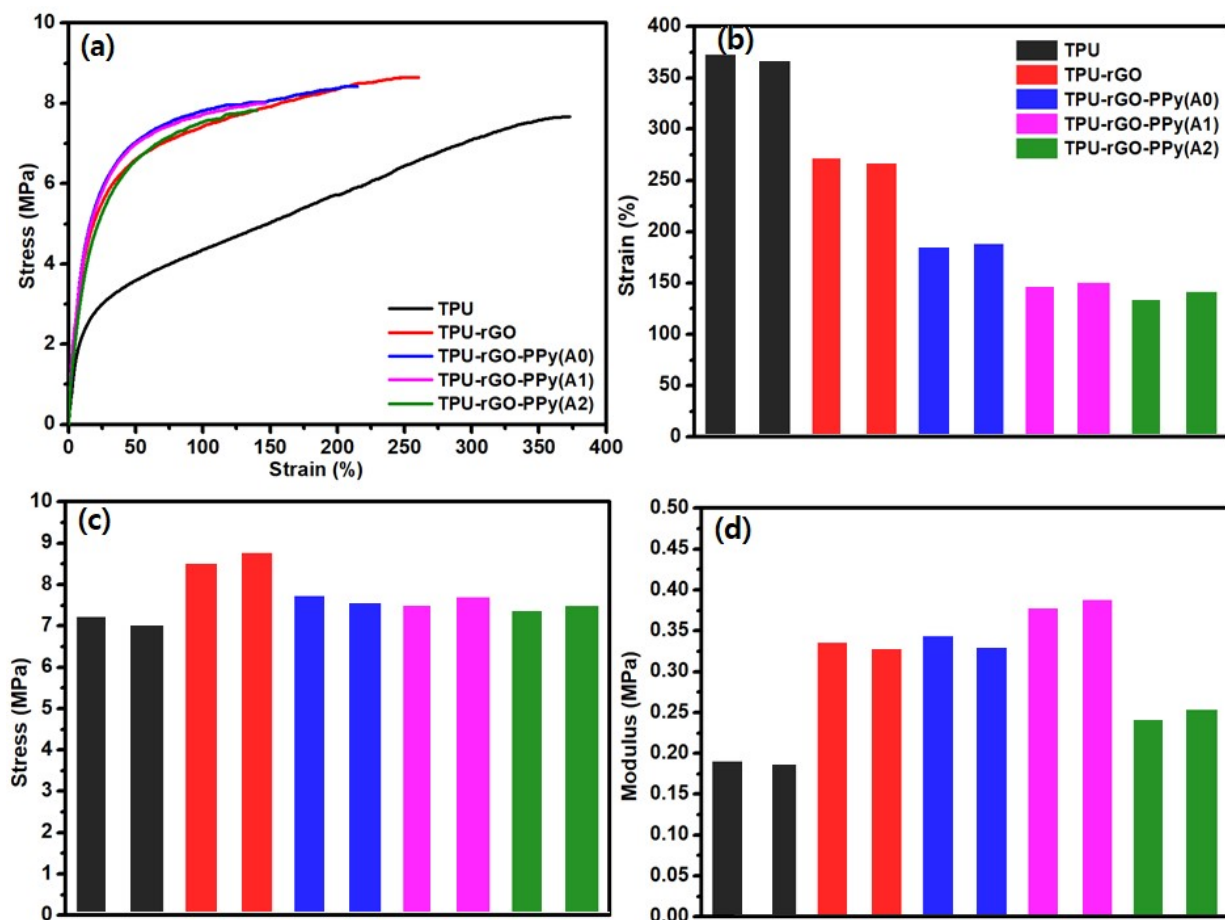


Fig.S3. Mechanical properties of the TPU-rGO-PPy composite films: (a) s-s curve, (b) max. strain, (c) max. stress, and (d) Young's modulus

Tab. S2. Mechanical properties of the TPU-rGO-PPy composite film

SAMPLE	STRAIN AT MAX (%)	MAX (MPa)	STRESS Young's (MPa)	modulus Electric conductivity (S/cm)
TPU	373.3	7.2	0.19	-
TPU/rGO	271.9	8.8	0.34	2.1
TPU/rGO/PPy(A0)	188.6	7.7	0.34	6.7
TPU/rGO/PPy(A1)	150.8	7.7	0.39	8.4
TPU/rGO/PPy(A2)	141.7	6.8	0.25	10.8

2.5. Electrochemical analysis

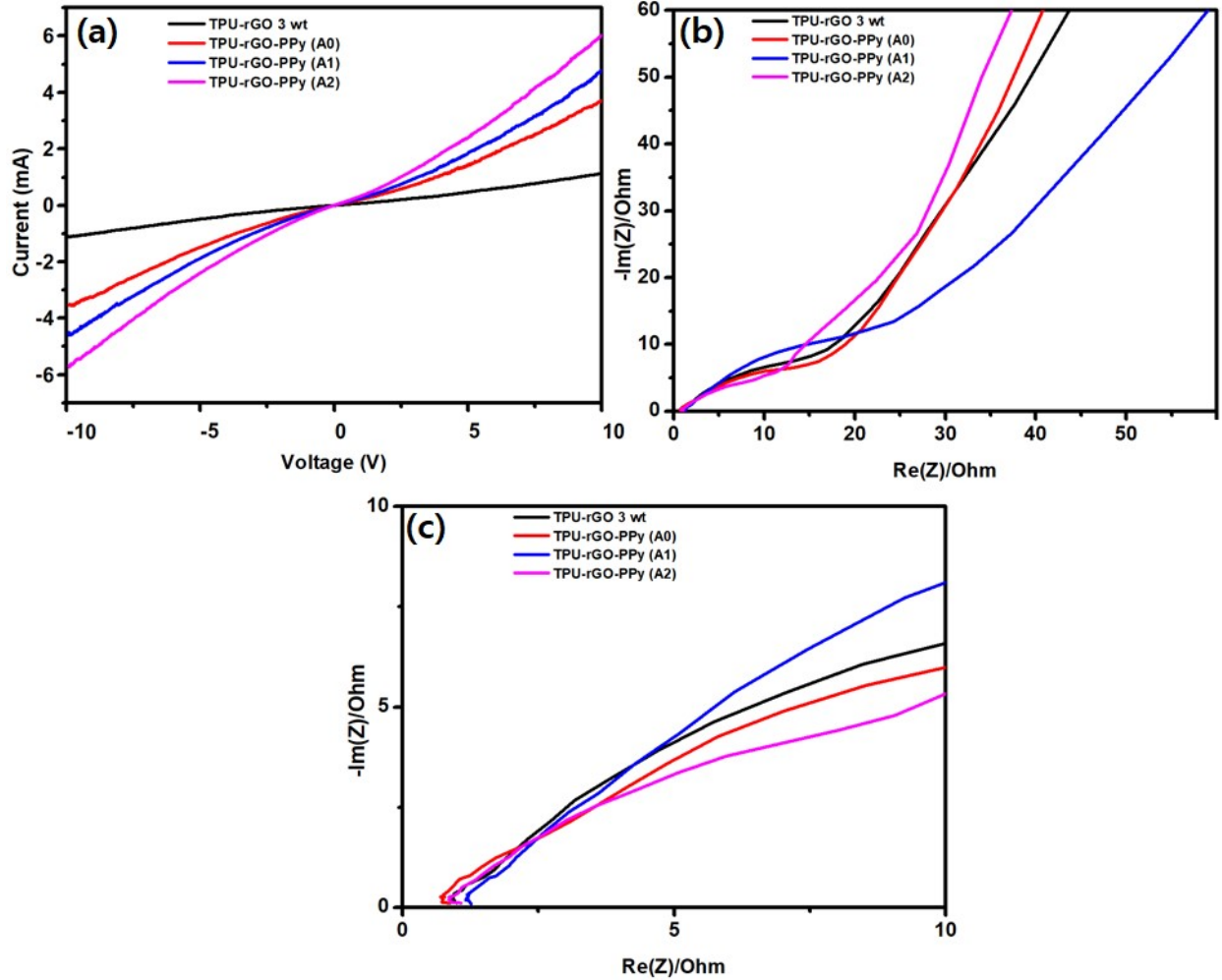


Fig. S4. I–V curves performance (a) and Nyquist plot: electrochemical impedance spectroscopy (b and c) of the TPU–rGO–PPy composite films.

The trend in which the relative resistance increased in a stepwise manner after the initial 20% and 60%, the electrical conduction path and chemical structure of the composite film deformed when a certain level or more of deformation occurred because TPU and rGO were secondarily bonded. The deformation of the electrical conduction path when extending to the 100% strain level did not reach the strain of the film length; thus, the change in the relative electrical resistance, following the elongation, was small. Similar to the previous result the highest change in the relative electrical resistance was observed when only rGO was utilized for continuous height deformation of up to 100%; furthermore, when A2 is

utilized, the electrical conduction interface broke, and the electrical resistance was not detected. The change in the width of the relative electrical resistance of the TPU-rGO-PPy composite film increased in the following order: rGO > A0 > A1 > A2, when the 10% strain-level 5000 elongation/contraction changes were applied. When only rGO added condition, the extension/contraction change was relatively irregular, and the overall relative electrical resistance value increases. When PPy added step, the electrical conductivity path and electrical resistance were stabilized. When A2 is utilized, it was suitable to utilize A0 for the strain sensors since it exhibited the most constant width for the change in the relative electrical resistance, as well as high sensitivity, although it was stable from the start to finish, exhibiting a very low range of change in the relative electrical resistance.

Fig. S4(a) shows that all the four TPU-rGO-PPy composite films except the non-electric TPU one exhibited linear metal-specific I-V curves with slight curves in the low-voltage range; this slope increased as the alkyl length of the utilized oxidant increased. Regarding the analysis of the performance of the SC, a sandwich-type TPU-rGO-PPy composite film selected for the SSs fabrication with an area of 10 × 10 mm, and a Whatman filter paper was utilized as the separator. Figs. S4 (b, c) show the Nyquist plot, which was obtained via electrochemical impedance spectroscopy (EIS), for analyzing the charge transfer at the electrode/electrolyte interface, as well as the resistance of the TPU-rGO-PPy composite film. In the Nyquist plot (Fig. S4 (b)), A2 exhibited the steepest slope, WR; in Fig. S4 (c), the composite film comprising A0 exhibited the lowest value in the following order: A0 > A2 > rGO > A1. However, dissimilar to the results of the experiment, a small difference observed in Rs. All the composite films exhibited low ion-resistance values in the electrolyte, indicating that the electrons might very easily during charging and discharging cycles.

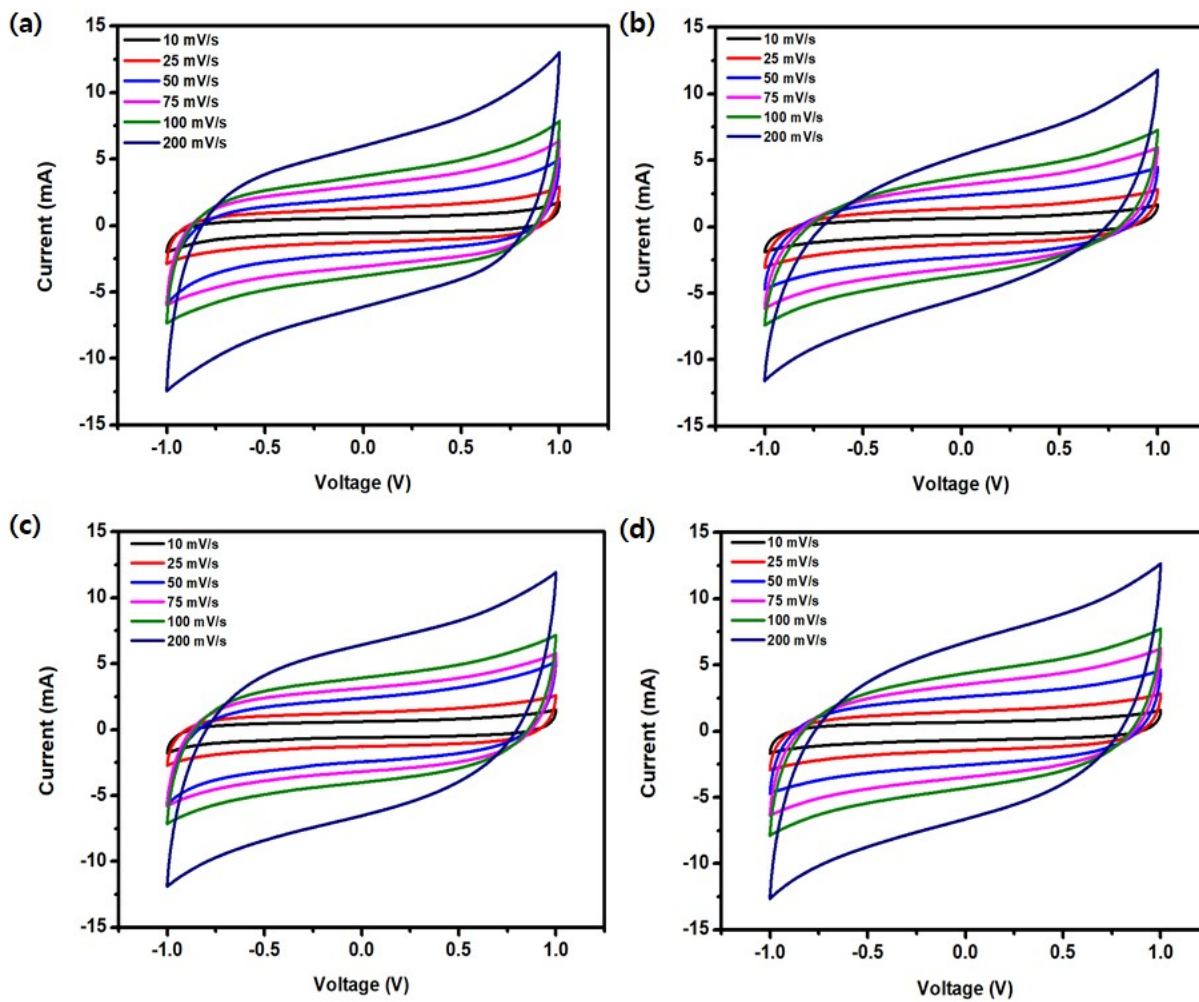


Fig. S5. CV profile of multi oxidant treated TPU/rGO/PPy composites films at various scan rates

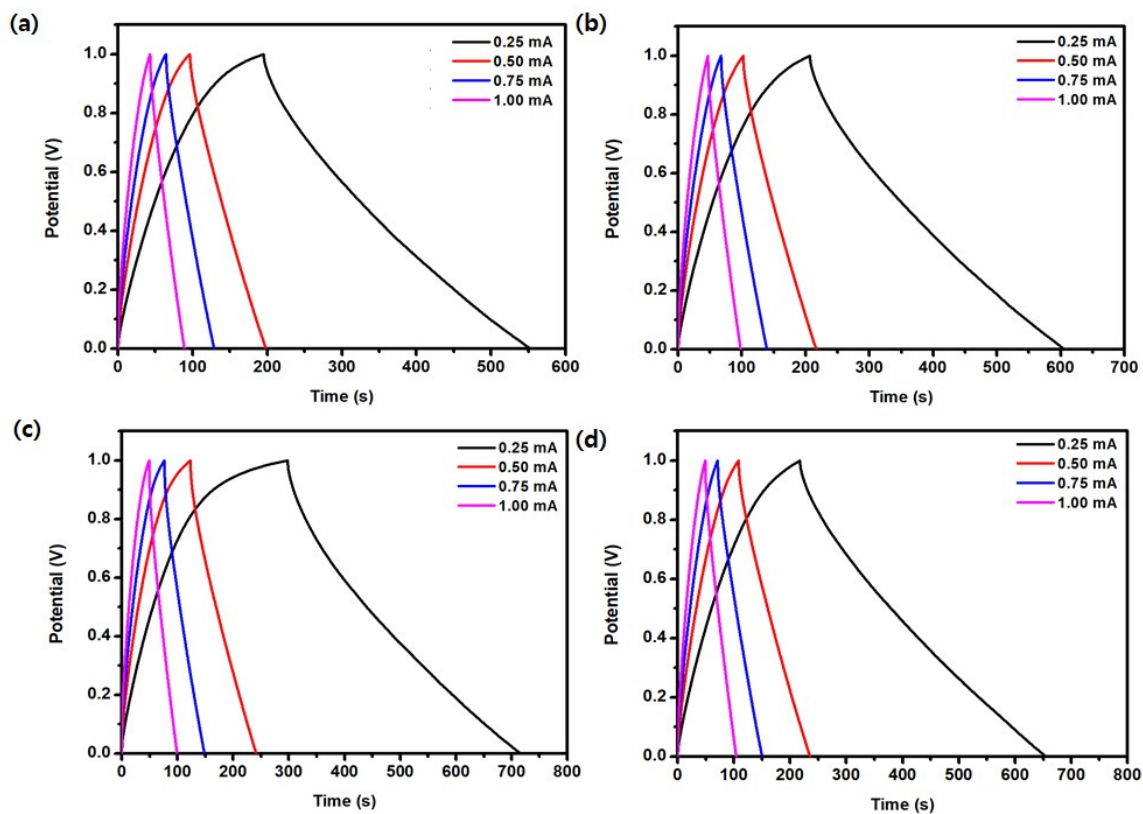


Fig. S6. GCD graphs of multi oxidant treated TPU/rGO/PPy composites films at various current densities

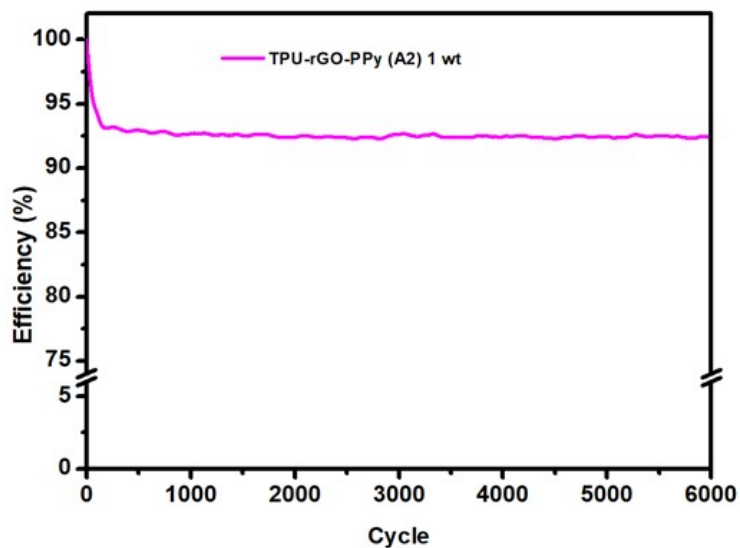


Fig. S7. Efficient long-term cyclic stability of the TPU-rGO-PPy(A2) composite films

2.6 Biocompatibility studies

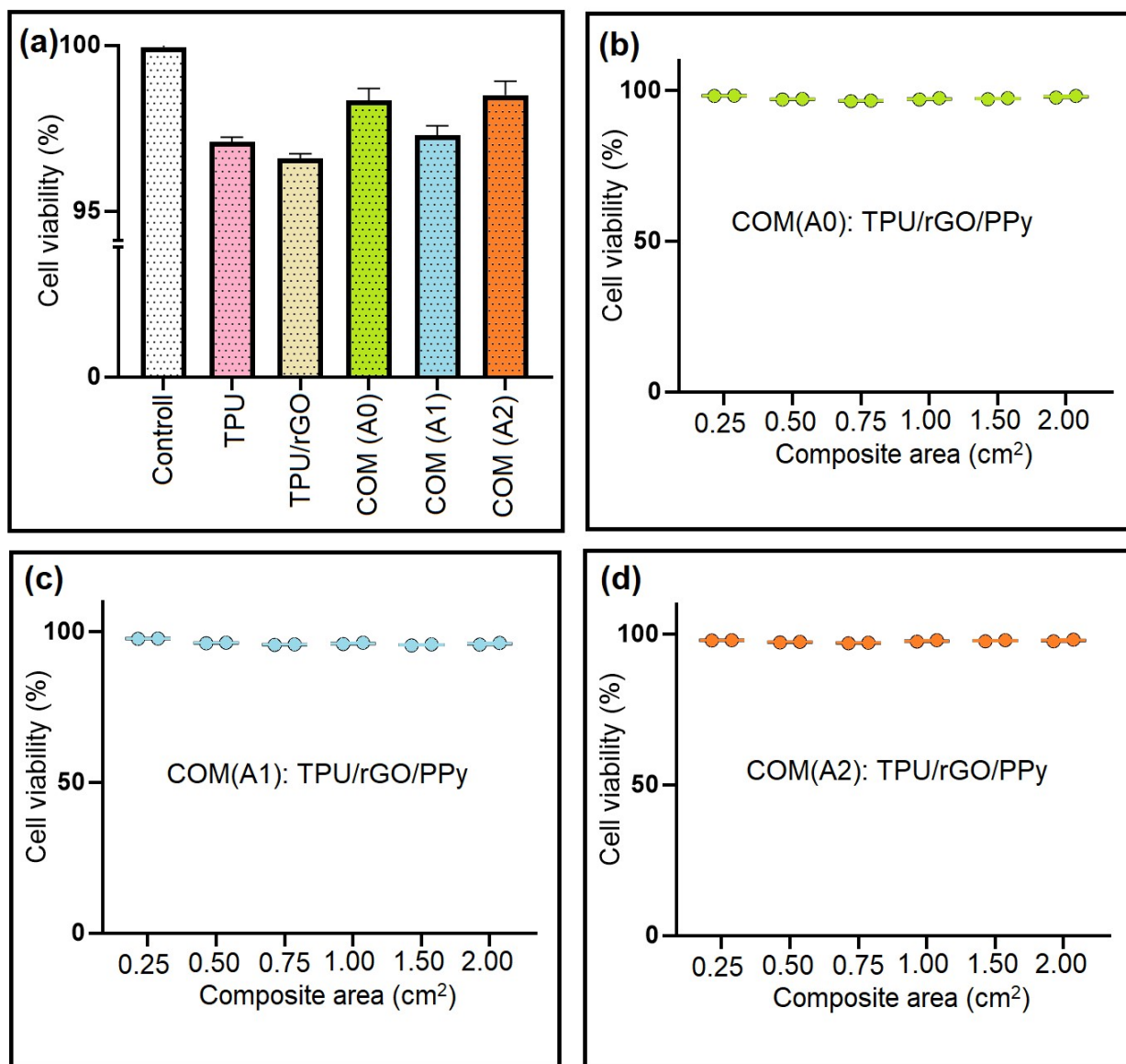


Fig. S8. Biocompatibility studies of TPU, TPU/rGO, TPU/rGO/PPy composites (a) and biocompatibility performances of A0 (b), A1 (c), A2 (d) TPU/rGO/PPy composites at different surface area respectively.

All the TPU, TPU/rGO, TPU/rGO/PPy multi oxidant treated samples were treated to conduct biocompatibility experiments on skin computability wearable sensor combined supercapacitors, and the findings are displayed in Fig. Treatment with HT-29 cells and composite films resulted in changes in cell

viability. The cell cultures (5×10^3 cells mL^{-1}) were grown in 24-well plates and preserved through IC50 (22.62 g mL^{-1}) in all the samples investigated using HT-29 cells in brief, the cell cultures (5×10^3 cells mL^{-1}) were cultivated in 24-well plates and preserved through IC50 (22.62 g mL^{-1}). After 24 h of growth, the cell viability fluctuations were observed using an inverted light microscope (Nikon, Eclipse TS 100). The obtained MTT assay against HT-29 cell line performances and Cell viability changes of HT-29 cells observed results demonstrated the notable good biocompatibility of TPU/rGO/PPY film and the various oxidant surface treated film influences on cell viability observed.

2.7. Comparative analysis from literature

Table S3. Comparative studies of TPU based composite strain sensors under various TPU configurations from literature.

TPU composite strain sensors	TPU Configurations	Detection range (%)	Cycles	Ref.	Performances
TPU/rGO/PPy (A2)	Film	10-100%	5000	This work	Supercapacitor-Strain sensor
CNT/TPU	Fiber yarn	50-140%	1250	1	Strain sensor
Graphene/TPU	Intertwined-Coil	>150%	1000	2	Strain sensor
PANI/TPU	Nano fiber	>160%	2000	3	Strain sensor
Ag/TPU	Nano wire	50-60%	2000	4	Strain sensor
Carbon Black/TPU	Fibrous Film	0-160%	10,000	5	Strain sensor
Ti ₃ C ₂ /ETPU	Electrospinning film	<50%	1000	6	Strain sensor
CNT/MXene-TPU	Skeleton mat	>50%	2600	7	Strain sensor
CNTs/MXene-TPU	Fiber	>50%	50	8	Supercapacitor-Strain sensor
BNNS/TPU	Fiber	100%	5000	9	Strain sensor
GNR/TPU	Electrospun Fiber	100%	5000	9	Strain sensor
MWCNT/TPU	Film	50%	50	10	Strain sensor
Ag NW/Ag flake/TPU	Composite ink	0-10%	200	11	Strain sensor

BNNS: boron nitride nanosheets; GNR: graphene nanoribbons;

2.8. Calculations

Capacitance could also be calculated from the galvanostatic discharge curves, using the following equation S1.

$$C = \frac{I\Delta t}{m\Delta V} \dots S1$$

Where I (A) is charge or discharge current, Δt (s) is the time for a full charge or discharge, m (g) indicates the mass of the active material, and ΔV represents the voltage change after a full charge or discharge.

Where C is the specific capacitance of the active materials, and ΔV is the potential window of discharge.

References

1. J. Tang, Y. Wu, S. Ma, T. Yan, Z. Pan, *Compos . B: Eng*, 2022, 232, 109605
2. W. Pan, W. Xia, F.-S. Jiang, X. -X. Wang, Z. -G. Zhang, X. G. Li, P. Li, Y.-C. Jiang, Y. Z. Long, G. -F. Yu, *Nanomat*, 2020, 10, 1980
3. L. Tong, X. -X. Wang, X. -X. He, G. -D. Nie, J.Zhang, B. Zhang, W. -Z. Guo, Y. -Z. Long, , *Nanoscale Res. Lett.* 2018, 13, 86
4. R. Wang, W. Xu, W. Shen, X. Shi, J. Huang, W. Song, , *Inorg. Chem. Front.*, 2019,6, 3119
5. X. Wang, X. Liu, D. W. Schubert, *Nano-Micro Lett.* 2021, 13, 64
6. B. Zhao, H. Cong, Z. Dong, *Smart Mater. Struct.* 2021, 30, 095003
7. H. Dong, J. Sun, X. Liu, X. Jiang, S. Lu, *ACS Appl. Mater. Interfaces*, 2022, 14, 13,
8. G. Wu, Z. Yang, Z. Zhang, B. Ji, C. Hou, Y. Li, W. Jia, Q. Zhang, H. Wang, , *Electrochim Acta*, 2021, 395, 139141
9. C. Tan, Z. Dong, Y. Li, H. Zhao, X. Huang, Z. Zhou, J. -W. jiang, Y. -Z. Long, P. Jiang, T.-Y. Zhang, B. Sun. *Nat. Commun.* 2020, 11, 3530.
10. S. Kumar, T. K. Gupta, K. M. Varadarajan, *Compos. B. Eng.* 2019, 177, 107285
11. M. M. Ali, D. Maddipatla, B. B. Narakathu, A. B. Chlaihawi, S. Emamian, F. Janabi, B. J. Bazuin, M. Z. Atashabar, , *Sens. Actuator A Phys.*, 2018, 274, 109.